2024 IEEE International Conference on Wireless for Space and Extreme Environments (WiSEE) | 979-8-3503-5111-8/24/$31.00 ©2024 IEEE | DOI: 10.1109/WiSEE61249.2024.10850420

Wi-Fi Signal Survey of the International Space Station by Autonomous Free-Flying Robot

Everest Yang[1], Shian U. Hwu[2], Chatwin Lansdowne[3], John P. Boster[4], Kanishka deSilva[5]

[1]Avionic Systems Division, Johnson Space Center, NASA, everest.yang@nasa.gov
[2] Barrios Technology, JET2/Jacobs/JSC/NASA, shian.u.hwu@nasa.gov
[3]Avionic Systems Division, Johnson Space Center, NASA, chatwin.lansdowne@nasa.gov
[4]Relative Dynamics, JET2/Jacobs/JSC/NASA, john.p.boster@nasa.gov
[5]Aerodyne Industries, JET2/Jacobs/JSC/NASA, kanishka.desilva@nasa.gov

***Abstract*— This paper analyzes Wi-Fi signal propagation inside pressurized modules of the International Space Station (ISS). Various flight datasets were collected by the Astrobee fleet of autonomous free-flying robots developed by the NASA Ames Research Center (ARC). The enclosed module spaces of the ISS pose unique challenges for Wi-Fi signal propagation, and understanding these challenges is crucial for optimizing connectivity in such environments. The survey data presented are valuable for optimizing wireless access point (WAP) locations and conditions. A computational method is developed to analyze the wireless communication system, RF coverage, and module compositions. The method is both rigorous and practical for assessing the ISS wireless system performance. The computational tools in this paper serve as a complementary approach to direct, on-orbit measurements, which is a complicated and expensive task. In some operational scenarios, ground measurements may be intractable due to the size of the spacecraft. Results from this research will aid future space missions and commercial spacecraft, providing insights into optimal WAP placements and robust wireless communication systems.**

Keywords*— *International Space Station, Astrobee, autonomous robot, Wi-Fi; Space exploration; Space communications; Space vehicles; astronaut; wireless LAN; multipath; propagation; communications; avionics

I. Introduction

In the age of ubiquitous connectivity, Wi-Fi has become an essential component of current and future spacecraft for human space exploration. It enables crews to access information, communicate, and engage with digital services effortlessly. However, the propagation of Wi-Fi signals can be influenced by the environment in which they operate. Optimizing Wi-Fi connectivity in spacecraft modules serves as a challenge. This paper explores the intricacies of Wi-Fi propagation in enclosed spacecraft crew modules, highlighting factors that impact signal propagation.

The International Space Station (ISS) uses Wireless Local Area Networks (WLANs) to provide continuous LAN services to mobile astronauts carrying portable computers. Wireless LANs can provide a flexibility not offered by wired systems when astronauts carry portable computers in the Space Station zero gravity environment. The performance of mobile communication systems, such as wireless LANs, is greatly affected by the radio wave propagation between the transmitter and the receiver. Unlike wired communications that are stationary, wireless radio propagations are environment dependent. Therefore, it is necessary to thoroughly understand the propagation characteristics for system performance optimization and verification.

A realistic Wi-Fi coverage map is essential for enhancing the era of ubiquitous connectivity. An effective method for surveying coverage is therefore highly desirable. In this study, an autonomous free-flight robot was introduced to collect the Wi-Fi signal data inside the International Space Station (ISS) crew modules [1-3].

II. Astrobee

The Astrobee was developed by NASA to assist astronauts aboard the International Space Station (ISS) [4-6]. The Astrobee robots are small, autonomous, cube-shaped free-flying robots designed to perform a variety of tasks in a microgravity environment. They can operate independently or be controlled remotely from the ground. The Astrobee robots can aid astronauts with routine tasks, scientific experiments, and maintenance activities aboard the ISS, shown in Figure 1.

Figure 1. Astrobee assisting Canadian Space Agency astronaut aboard the International Space Station on Expedition 59.

Each Astrobee robot is equipped with a suite of sensors, cameras, and tools to navigate and interact with its surroundings. They have a 3D mapping system to navigate and

avoid obstacles, and their modular payload system allows for the attachment of different tools and instruments for various tasks. The antennas used in Astrobee are internal antennas integrated into the computing unit for the ISAAC payload.

Astrobee robots can fly freely in any direction and maneuver themselves to reach different locations within the Space Station. The ISAAC payload communicates with the ISS crew and the ground control center using Wi-Fi and a wireless network infrastructure installed on the station. The robots also serve as a platform for testing new technologies and algorithms for future space exploration missions.

III. Flight Data

The International Space Station (ISS) consists of many modules, which are metallic, cylindrical structures. Each module is connected by a closeable hatch, allowing crew members to move freely between different modules. The enclosed space and the one-dimensional extension make the Space Station modules a very unique propagation environment.

The enclosed module environments could cause RF signal reflections that change the signal distribution inside the modules. Hence, the signal strength may be modified due to the constructive and destructive interference among direct and reflected RF signal components.

Numerical data were collected by the ISAAC payload during various operations conducted by the Astrobee robots. Selected, representative surveys were analyzed from Astrobees "Queen" and "Bumble" in the US Laboratory (US Lab) and Japanese Experiment Module (JEM). On the ISS, the US Lab and JEM are connected by a pressurized module and Node 2. The performance of the Wi-Fi radio and antennas in the ISAAC payload were not characterized before flight. ISAAC connects to 2.4GHz and 5GHz networks on the ISS.

A complete set of results is given in the technical report [1]. Figure 2a. shows the WAP inside Node 2 onboard the ISS, which is located at the corner of the JEM and US Lab modules, as shown in Figure 2b. Astrobee traveling paths are shown in Figure 2c. Figure 2d. represents all the signal survey data used in this paper plotted on a composition diagram of the ISS [1].

Figure 2a. BelAir WAP mounted near the hatch in Node 2. Photo taken during Expedition 36.

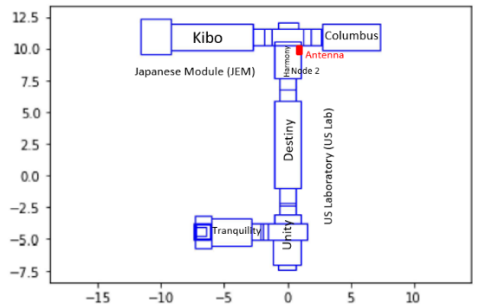

Figure 2b. The WAP antenna is located at the corner of the JEM and US Lab modules (Top View).

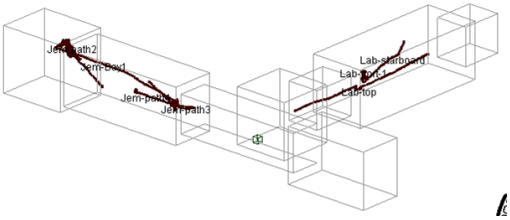

Figure 2c. The selected Astrobee traveling paths during the signal survey campaign.

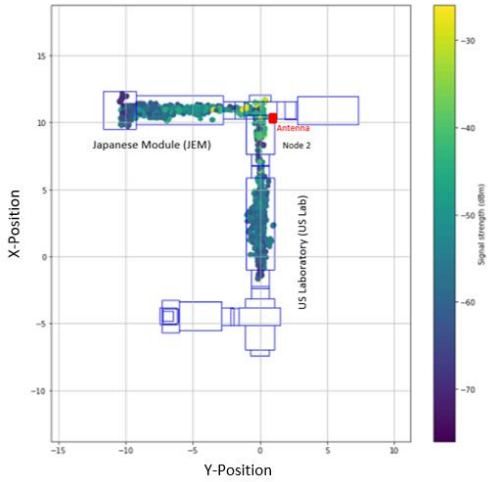

Figure 2d. Astrobee signal survey visualization over ISS configuration. Credit: NASA Ames Research Center.

In this study, signal survey data of the US Lab and JEM modules from 2022 were used to analyze signal propagation and RF coverage. The Astrobee data were precisely collected in epoch time to the nanoseconds. Astrobee's X, Y, Z cartesian coordinates and orientations were determined optically, and tracked along with the respective Wi-Fi signal strength. Experiments were conducted in various modules, Node 2, and hatches. Note, the X-axis increases toward the fore of the ISS vehicle, the Y-axis increases to starboard, and the Z-axis increases toward the center of the Earth. Figure 2 uses standard Space Station coordinates. In the data sets ISAAC was connected to a single WAP located in Node 2.

IV. Methodology

A computational approach was developed to rigorously analyze the data collected by the Astrobees. The WAP is located inside a mixed-conductivity rectangular corridor within a

conductive cylinder which indicates the free space pathloss model (~$1/R^2$ where R is the distance from the antenna) is invalid. Though the direct signals from the antennas are with $1/R^2$ pathloss, the indirect signal components such as the reflections off the walls are geometry and materials dependent. This results in a much more complex pathloss model.

Part A. Position vs. Signal Strengths

To visualize trends as a whole, a 3D model of the X, Y, Z positions versus their respective signal strengths inside the US Lab overhead, as shown in Figure 3.

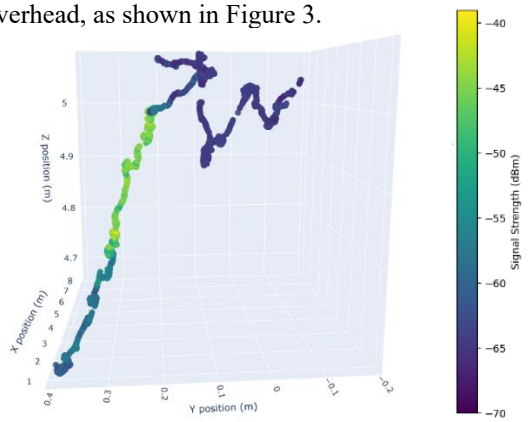

Figure 3. X, Y, Z positions where color denotes signal strength along a path inside US Lab module.

As seen, there is a notable trend where the signal in particular positions is stronger than others, where signal strength can jump 20 dB (from -65 dBm to -45 dBm). It is important to note that narrower pathway space could affect the number of signal bounces. In this dataset, the optimal coordinate positions range from (1.89m, 0.30m, 4.82m) to (3.98m, 0.22m, 4.99m) for the best signal propagation.

Similarly, Figure 4 showcases a point cloud of 3D data across several datasets from the JEM module, which were collected across several runs by both Astrobees. Again, there is a notable trend where the signals in particular clusters are stronger than others, ranging from approximately -45 dBm to -60 dBm. The clusters with stronger signal strengths (green) are closer to the WAP compared to the weaker signal strengths (blue) which are further away—this makes sense intuitively and supports Figure 3 from above.

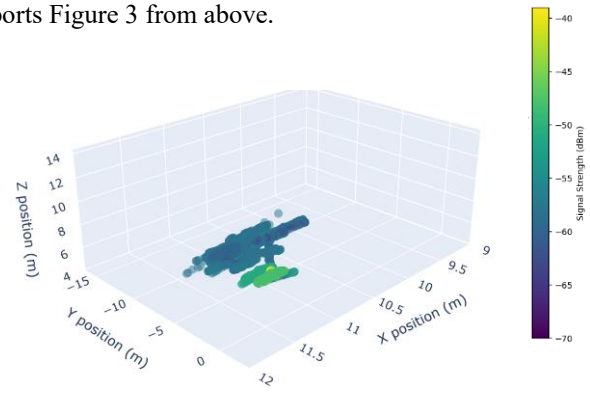

Figure 4. X, Y, Z positions where color denotes signal strength along a path inside JEM module.

As noted above, the free space pathloss model/inverse squared law (~$1/R^2$ where R is the distance from the antenna) is not valid in an enclosed module environment. Some areas have strong reflections while others do not, so the signal levels and pathloss models will be different. An empirical model may not be practical for including these geometrically dependent variations. Therefore, a deterministic model based on computational electromagnetic methods and assumptions as well as measurements of material properties and operational configurations is required.

This paper examines the candidate exponential form, Power $\propto 1/R^b$, as a fading model. The exponent "b" is determined by analyzing the slope of the relationship between the logarithm of Euclidean distance and corresponding signal strengths. The computational model is shown in Figure 5.

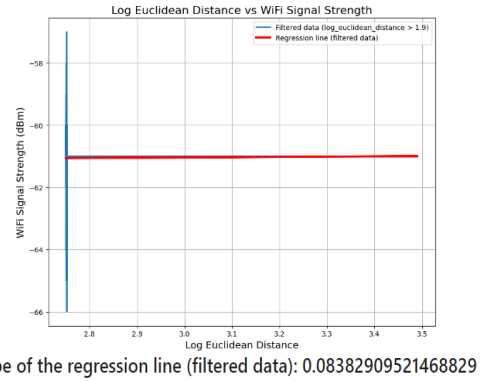

Figure 5. Signal strengths versus Log Euclidian Distance along a path inside JEM module.

As seen in Figure 5, the slope is 0.084 which is essentially flat for the JEM and it is the same case for the US Lab. This means in the US Lab, the X-axis (longitudinal axis of the module) can be cross sectioned. Since changes along the longitudinal axis position do not significantly affect the power received in these modules, this paper compares how signal strength is affected by the relationship between the Y-position and Z-position. Thus, the Y and Z position coordinates are translated to originate at the actual location of the BelAir WAP in Node 2, and a heatmap is graphed below, shown in Figure 6.

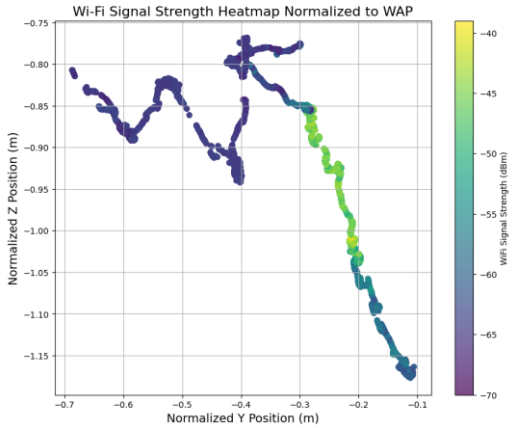

Figure 6. Signal Strength of normalized Y-position versus normalized Z-position in US Lab, relative to the WAP.

As seen, there is a clear trend following a similar shape from the figures above. The data shows a movement in Y and Z position, where signal strength can jump 12 dB (from -60 dBm to -48 dBm). The signal is optimized when -0.3m < Y < -0.2m and when -1.03m < Z < -0.85m, excluding the dip of outliers for the Z position. This means the best location for propagation relative to the WAP is roughly 1 meter above the transmitting antenna, and slightly to the left as viewed in Figure 2a.

This paper also investigates the signal strength in relation to the proximity of the receiving antenna to the center of the module and metal wall. Thus, the 3D position is translated to originate at the at the centerline of the USLab. Then, the relationship between the Y-position and Z-position is graphed, shown in Figure 7a.

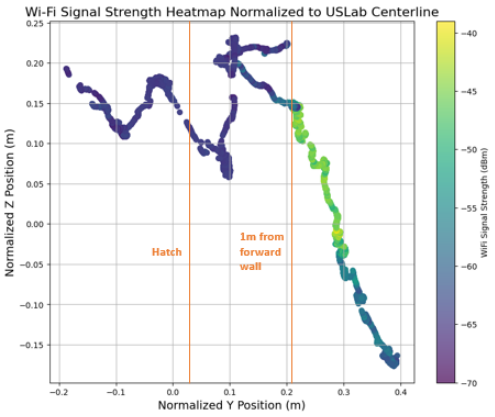

Figure 7a. Signal Strength of normalized Y-position versus normalized Z-position in US Lab, relative to the centerline.

The WAP is situated to the right of the USLab's centerline facing forward, which is closer to the wall. Furthermore, a hatch located between the WAP and the centerline contributes to the slightly weaker signal observed between 0.27m < Y < 0.4m. On the left side of the graph, the signal deteriorates significantly. This is due to Astrobee collecting data near the ends of the module, very close to the wall borders. By filtering out X > 5.5m, which is the hatch between USLab and Node 2, most data points with poor signal strength are excluded, as illustrated in Figure 7b. Moreover, the signal strength drops significantly near 1m from the forward wall of the USLab.

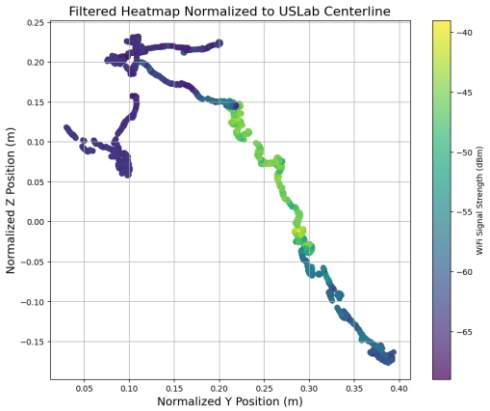

Figure 7b. Filtered Heatmap of Figure 9a with X > 5.5m.

Thus, the consensus is that signal strength tends to be stronger when closer to the centerline and further from the metal walls. However, to examine the weaker signal and explore the outlying data further, this paper uses the Rician Distribution, which is widely utilized in wireless communications to model signal propagation environments. This statistical distribution is particularly effective in scenarios where there is a predominant direct line-of-sight path between the transmitter and receiver, accompanied by multiple scattered and reflected paths. The Rician Probability Distribution Fit (PDF) is denoted as:

$$f(x \mid \nu, \sigma) = \frac{x}{\sigma^2} \exp\left(-\frac{x^2 + \nu^2}{2\sigma^2}\right) I_0\left(\frac{x\nu}{\sigma^2}\right)$$

where $x \geq 0$, $\nu \geq 0$, $\sigma > 0$, and I_0 is the modified Bessel function of the first kind with order zero.

The signal strength is currently expressed in decibels relative to one milliwatt (dBm), which uses a logarithmic scale. However, the Rician Distribution requires signal measurements to be on a linear scale for accurate modeling. Thus, signal strength values are converted from dBm to watts to meet this requirement. When the signal strength is graphed against density with the US Lab overhead data, it does not fit well under the Rician Distribution function, as shown in Figure 8a. This indicates a possible discrepancy between the modeled distribution and the actual signal characteristics observed in the data set. It is important to note that the data is quantized in 1dB steps, which is why the graph shows bins.

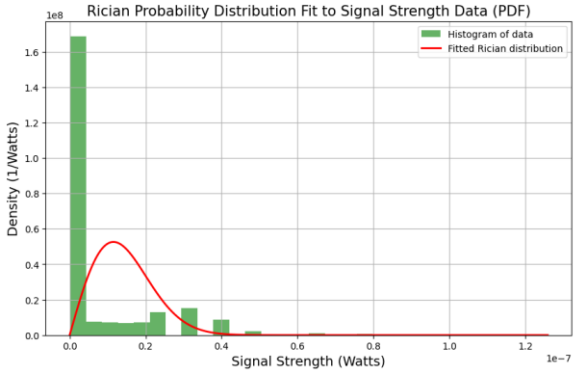

Figure 8a. Rician Probability Distribution Function fitted over Signal Strength Histogram.

To investigate this discrepancy further, signal strengths below 0.1 * 10^{-7} are excluded and plotted using the Rician Cumulative Distribution (CDF) in Figure 8b. The CDF, being the integral of the Probability Density Function (PDF), offers several advantages, such as determining percentiles. CDF is denoted as:

$$\int_0^r f_R(t)\, dt$$

where $f_R(t)$ represents Rician PDF and r is the upper bound limit of R

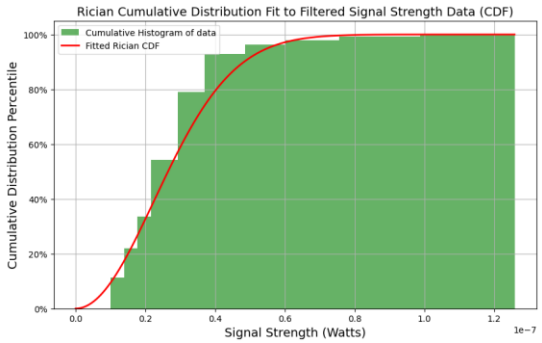

Figure 8b. Filtered Rician Cumulative Distribution Function fitted over Signal Strength Histogram.

As seen, the cumulative histogram of the data aligns closely with the Rician PDF, indicating that there was an anomaly observed in the signal strengths below 0.1 * 10^{-7} watts on the ISS. However, after several tests including Rayleigh's distribution (where the shape factor of Rician distribution is near 0), this study confirms that the jump is not due to Astrobee switching between 2.4GHz and 5GHz radios, as results were repeatable between sorties and between Astrobees Queen and Bumble. Additionally, while the presence of an astronaut in the module may have some measurable effect on signal strength, it is unlikely to result in a reduction as substantial as 20 dB.

This paper hypothesizes that the signal degradation may have been caused by storage racks or other material obstructions. Given the constraints of this dataset, further targeted research is necessary to better understand signal propagation in proximity to module walls.

Part B. Orientation vs. Signal Strengths

The signal surveys conducted by Astrobee also included 3D orientation during the collection of signal strength measurements. This paper aims to discover any potential relationship between orientation and signal strength. However, despite extensive testing and visualization efforts, the results indicate no discernible relationship between Astrobee's orientation and received signal strength. Both 2D and 3D computational models exhibited random trends that failed to reveal any significant correlation.

In most cases, adequate signal strengths were observed inside the modules. Signal levels in some isolated locations were lower than the threshold levels due to severe, destructive multipath fading. The standing wave phenomenon is observed in some locations. The peaks and valleys could be shifted for different channel frequencies. The Wi-Fi system could improve localized poor coverage by switching to a different channel.

Since monopole antennas (linear polarized) are widely used in commercially available Wi-Fi devices, this paper investigates that relative antenna orientations may be important for certain scenarios. The orthogonal orientation (90-deg angle between the access point antenna and the client Wi-Fi antenna) is the worst case. Orthogonal or near orthogonal antenna orientation could result in a signal drop of approximately 20 dB or more as depicted in Figure 9. Better signal level and link performance can be achieved by arranging the access point antenna and the client/user's antenna pointing in the same direction (parallel to each other). This is denoted by the relationship between polarization loss and misalignment angle, shown in Figure 9.

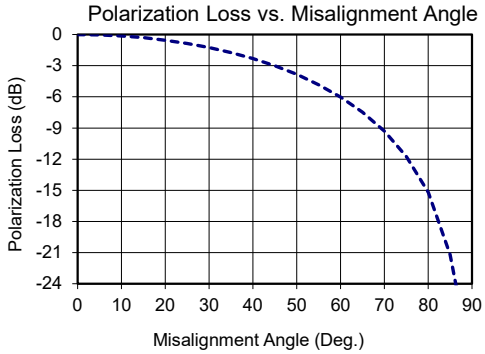

Figure 9. Polarization loss versus antenna misalignment angle between two linear polarized antennas.

Part C. Node 2 and Hatch Signal Strengths

Given that the WAP is located inside Node 2, the received signal strength is expected to be optimal when inside Node 2, assuming direct line-of-sight conditions. When there are minimal obstructions hindering the signal path, the propagation is anticipated to be the strongest, as shown in Figure 10. Factors such as the presence of personnel or ongoing experiments within Node 2 may affect signal strength due to potential transient or variable blockage in usage patterns. Despite the unique environment of the ISS, fundamental principles governing wireless communication within the ISS structure remain applicable. Note the lower negative dBm scale of the color-bar key for Figure 10 – it has different limits compared to previous figures because the signal is generally much stronger.

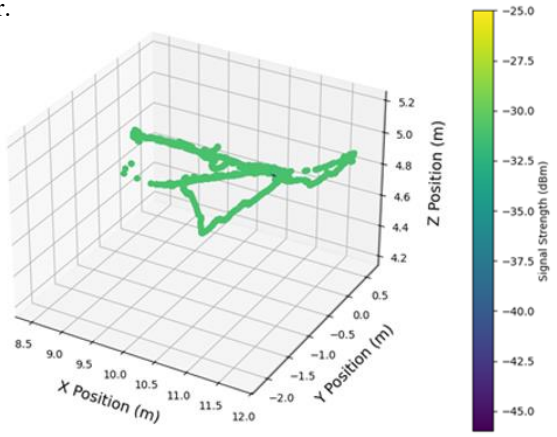

Figure 10. 3D Scatterplot of Position versus Signal strength inside Node 2.

This paper also examines the signal strength of hatches between modules on the ISS. It's important to focus on the differences in power levels observed during tests rather than absolute power levels, particularly in various conditions such

as when hatches are open. Unlike open spaces within individual modules, signal propagation through hatches is significantly hindered by their design. The narrower hatches introduce substantial signal attenuation, resulting in poorer signal reception compared to open module environments, as shown in Figure 11. Note the higher negative dBm scale of the color-bar key – it uses different limits compared to previous figures because the signal is generally worse.

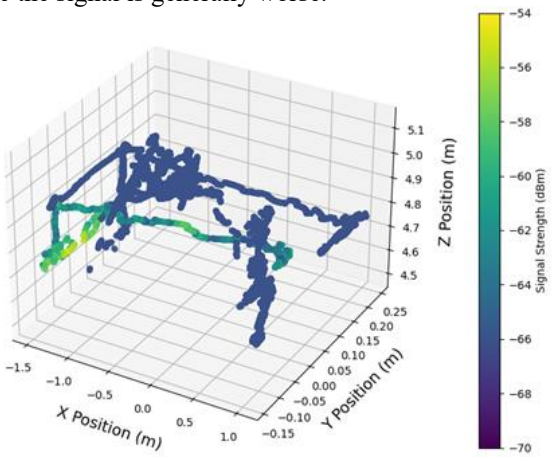

Figure 11. 3D Scatterplot of Position versus Signal strength inside a hatch between US Lab and JEM.

V. Discussion

Due to the reflections off metallic surfaces, RF signals arrive at a WAP with different strengths, phases, and polarization. Thus, a receiver at one location may have a signal strength that is quite different from a similar receiver located only a few inches away. When an astronaut moves from one location to another, significant signal fluctuations may occur depending on the surrounding environment.

The conventional $1/R^2$ pathloss roll-off is not valid in spacecraft module environments. Along the center of the module, the pathloss exponent was near zero. Significant signal changes could occur due to reflection boundary or segmentation effects. Signals could drop due to structural blockage effects.

Positioning the Wi-Fi router in an optimal location within the enclosed environment is essential. It is recommended to place the router away from physical obstacles and sources of interference such as metallic objects and hatches. Adjusting the layout, and avoiding reflective bodies in close proximity to the antenna can help reduce signal fading.

Wi-Fi operates on different frequency bands, with multiple channels available within each band. In crowded environments, selecting the optimal Wi-Fi channel can reduce interference from neighboring networks. Wi-Fi routers may offer automatic channel selection, as selecting a less congested channel can significantly improve signal quality and overall performance.

In multiple interconnected module environments, network segmentation can be beneficial. By dividing the network into smaller, localized subnets, each with its own router, interference and congestion can be minimized. This approach ensures better signal propagation and reduces the likelihood of overcrowded Wi-Fi channels.

VI. Conclusion

Wi-Fi propagation in enclosed environments such as spacecraft present unique challenges due to physical obstacles, signal interference, and reflection effects. This paper explores the intricacies of Wi-Fi propagation in operational space station modules, highlighting factors that impact signal propagation. Signal strength decreased along the length of the module's axis, following an inverse power law with a distance exponent of 0.084, very low propagation loss. However signal strength reduces with distance from the center of a module, and a significant signal drop of 35 dB was recorded when crossing through hatches. Furthermore, regions within the modules were identified where signal attenuation reached up to 15 dB in pathloss. By employing strategies such as optimal router placement, antenna diversity, channel selection, reduction of signal reflections, and network segmentation, the connectivity within these spaces can be greatly enhanced.

Acknowledgment

The authors would like to thank Trey Smith, Jose V. Benavides, and Jonathan S. Barlow, NASA Ames Research Center (ARC) for providing the Astrobee Wi-Fi Data Packages and for their valuable feedback and comments.

References

[1] Trey Smith, Jose V. Benavides, Jonathan S. Barlow, "Astrobee Wi-Fi Data Packages," NASA Ames Research Center (ARC), April 17, 2023

[2] Aric Katterhagen, Jose Benavides, Maria Bualat, Trey Smith, Andres Mora, Jonathan Barlow, and Roberto Carlino, "Current and Future Science using Free Flying Robots on the ISS - The Astrobee Facility and Research Opportunities," In Proc. Int. Space Station Res. Dev.s Conf. (ISS-RDC), 2022.

[3] Jonathan Barlow, Trey Smith, Jose Benavides, Maria Bualat, Aric Katterhagen, Ernest Smith "Astrobee: A Free Flying Robot Enabling Technology Demonstrations," In Proc. Int. Space Station Res. Dev. Conf. (ISS-RDC), 2021.

[4] Nicoletta Panunzio, Cecilia Occhiuzzi, Gaetano Marrocco, "Propagation Modeling Inside the International Space Station for the Automatic Monitoring of Astronauts by Means of Epidermal UHF-RFID Sensors", IEEE Journal of Radio Frequency Identification, vol.5, no.2, pp.174-181, 2021.

[5] A. Di Carlofelice, E. Di Giampaolo, P. Tognolatti, "A numerical investigation of UWB wave propagation inside a module of the International Space Station", International Symposium on Electromagnetic Compatibility - EMC EUROPE, pp.1-6, 2012.

[6] Norman Lay, Clayton Okino, Arby Argueta, Kris Bruvold, Neil Chamberlain, Daniel Cho, Colin McKinney, Greaory Miles, Pablo Narvaez, Charles Rhoades, Ryan Rogalin, Manuel Soriano, William Walsh, Yu-Ming Yang, "On-Board Wireless Communications for Spacecraft Test and Operations", 2019 IEEE Aerospace Conference, pp.1-16, 2019.